Radiation loss of photonic crystal coupled-cavity waveguides

J. Jágerská,[a] H. Zhang, N. Le Thomas, and R. Houdré
Institut de Photonique et d'Electronique Quantiques, Ecole Polytechnique Fédérale de Lausanne (EPFL), Station 3, CH-1015 Lausanne, Switzerland

(Received 26 June 2009; accepted 16 August 2009; published online 15 September 2009)

We experimentally investigate the out-of-plane radiation losses of photonic crystal coupled-cavity waveguides. We observe a strong variation in the losses along the dispersion curve and show that such variation is closely linked with the specific far-field radiation pattern of a single cavity constituent. A simple theoretical model based on tight-binding approximation is used to describe this behavior. © *2009 American Institute of Physics*. [doi:10.1063/1.3222905]

Photonic crystal (PhC) coupled-cavity waveguides (CCWs)[1,2] have recently raised a large interest in the field of slow-light engineering. Extremely low group velocity of the CCW mode along with nearly-zero group velocity dispersion allows for optical pulse retardation with negligible pulse distortion, which is highly desired in communication applications such as buffers or integrated optical delay lines. The eligibility of the CCW concept for practical use has been highlighted lately by Notomi *et al.*,[3] who reported a pulse delay as large as 125 ps in a device formed by 150 coupled cavities. However, the state of the art CCWs still suffer from high propagation losses, predominantly due to strong out-of-plane radiation from the concatenated cavities. Such radiation loss is inherent to two-dimensional (2D) PhC CCWs and has to be considered and efficiently managed in practical devices.

Recent theoretical work[4,5] has shown that the CCW radiation loss primarily depends on the quality-factor (Q) of a single cavity, but may vary substantially by several orders of magnitude along the dispersion curve. More specifically, the waveguide quality factor can be significantly higher or lower than the Q of the constituent cavities[4] and it changes as a function of the wave-vector $\vec{k}$ of the propagating mode. The physical origin of this variation can be partially explained by the light-line argument, i.e., the optical loss increases with the number of Bloch mode components lying in the light cone. However, this approach provides only a crude physical understanding.

In this letter, we will show that along with the number of Bloch modes lying inside the light cone, the magnitude and the wave-vector dependence of the CCW radiation loss is mainly determined by the far-field radiation pattern of an isolated cavity constituent. The relation between the single cavity radiation pattern and the CCW radiation loss will be explained theoretically using a simple analytical model based on the tight-binding approximation, and demonstrated experimentally on a chain of weakly coupled photonic crystal cavities.

The origin of the radiation loss of CCWs can be intuitively understood in terms of a finite mode lifetime of the constituent cavities. Optical cavities fabricated in 2D PhC slabs rely on vertical light confinement by total internal reflection, which is incomplete and allows the energy to leak out of the cavity leading to out-of-plane radiation loss. For the case of a single cavity (SC), it has been shown[6,7] that the total radiated power P_{SC} is related to the Fourier transform of the electromagnetic field right above the slab interface, and can be expressed as an integral over the spatial frequencies $(k_\perp, k_\parallel)$ lying within the light cone

$$P_{SC} \propto \int_{k<(\omega/c)} |E^{SC}(k_\perp,k_\parallel)|^2 dk = \int_{k<(\omega/c)} |\mathrm{FT}[E^{SC}(r_\perp,r_\parallel)]|^2 dk, \tag{1}$$

where ω stands for the resonant frequency of the cavity and c is the speed of light.

A similar approach can be used to estimate the radiation loss of the CCWs. As schematically shown in Fig. 1(a), we assume a finite CCW that consists of N cavities concatenated along the $r_\parallel$ axis, separated by a distance Λ. Within the tight-binding approximation, one can express the near-field pattern of the CCW as a linear combination of the eigenmodes $E^{SC}(r_\perp, r_\parallel)$ of individual cavities[2]

$$E_\omega(r_\perp,r_\parallel) = \sum_{n=-N/2}^{N/2} E^{SC}(r_\perp, r_\parallel - n\Lambda)e^{ik(\omega)n\Lambda}. \tag{2}$$

Such near-field distribution is an explicit function of the mode propagation constant $k(\omega)$, and it varies significantly with the frequency ω owing to the strong dispersion of the CCW slow mode. By performing the Fourier transform of

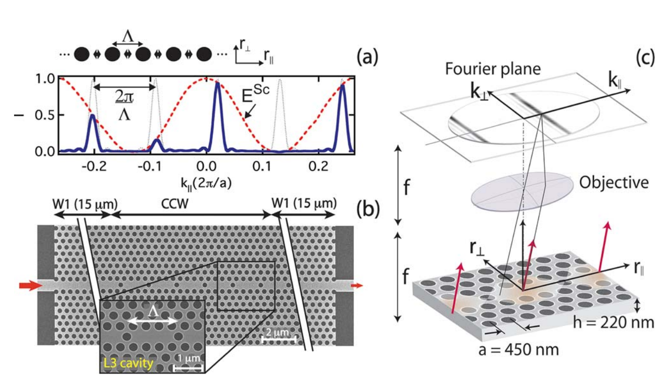

FIG. 1. (Color online) (a) Theoretical one-dimensional far-field spectrum (solid curve) of CCW with $\Lambda=9a$, $N=20$, and $k_0=0.02(2\pi/a)$. Single-cavity far-field pattern (dashed curve) that forms the envelope function of the CCW spectrum is also shown. Above: real-space layout of the CCW. (b) Top-view SEM image of the fabricated CCW including the access waveguide layout. (c) Fourier-space imaging setup.

[a]Electronic mail: jana.jagerska@epfl.ch.

$E_\omega(r_\perp, r_\parallel)$, the so-called far-field pattern of the CCW is obtained

$$E_\omega(k_\perp,k_\parallel) = E^{\mathrm{SC}}(k_\perp,k_\parallel) \times N \sum_{n=-\infty}^{\infty} \mathrm{sinc}\left[\frac{N\Lambda}{2\pi}\left(k_\parallel - k(\omega) - \frac{2\pi n}{\Lambda}\right)\right]. \quad (3)$$

Radiation loss of the CCW can be evaluated in the same way as for a single cavity, i.e., by integrating $E_\omega(k_\perp,k_\parallel)$ over all spatial components that lie below the light line.

An example of the theoretical far-field pattern of the CCW [Eq. (3)] is given in Fig. 1(a), which plots a one-dimensional far-field spectrum of a CCW formed by $N=20$ cavities with a periodicity of $\Lambda=9a$, with a being the lattice constant of the bulk photonic crystal lattice. The theoretical far-field pattern consists of a series of peaks, which are equidistantly spaced along the $k_\parallel$ axis and separated by the reciprocal vector of the coupled-cavity chain $|\vec{G}|=2\pi/\Lambda$. Since the coupled-cavity chain is limited in length, each of the peaks is further broadened by a sinc profile with a linewidth inversely proportional to the total length of the structure $L=N\Lambda$. In the limit of $N\to\infty$, i.e., for an infinitely long structure, the far-field pattern reduces to a comb of delta functions $\sum_{n=-\infty}^{\infty}\delta(k_\parallel - k - 2\pi n/\Lambda)$. Finally, the amplitude of individual peaks is determined by the emission pattern of an isolated cavity $E^{\mathrm{SC}}(k_\perp,k_\parallel)$, which acts as an envelope function modulating the whole CCW emission spectrum. The CCW mode can freely radiate only at those k-vectors at which a SC radiates, and in all other directions the radiation is suppressed. As a consequence, any inhomogeneity of the SC far-field pattern along the $k_\parallel$ axis results in a variation in the emission yield and, hence, the CCW loss along the dispersion curve.

There are interesting similarities between the present analysis and models used for optimization of blazed diffraction gratings[8] or phased antenna arrays.[9] In both cases, the generated far-field pattern can be expressed as a product of an envelope function describing a unit cell and a comb function generated by the periodicity. Though, the design goals are quite different: for a CCW, the purpose is to suppress all Bloch mode components inside the light cone for all frequencies of the mode bandwidth, in contrast to antennas or blazed gratings, where the suppression of all *but one* diffraction orders is desired. The free parameters and constraints differ also significantly. Blaze conditions are usually obtained by continuously tuning the relation between the period and the frequency, while for the CCW the period can only change by discrete values. On the other hand, the cavity mode and the coupling constant represent additional degrees of freedom to be controlled.

To experimentally illustrate the mechanism of CCW radiation loss, we have measured and compared the far-field patterns of both an isolated PhC cavity and CCW formed by a chain of $N=20$ identical cavities. As can be seen in Fig. 1(b), each cavity is created by removing three holes along the Γ-K direction (so-called L3 cavity) and is separated from the neighboring cavities by one adjacent hole. The experimental Q-factor of the constituent cavities was found equal to 4500. The lattice constant $a=450$ nm and the filling factor of $f=0.4$ were chosen such that the fundamental cavity mode lies within the 1.5 μm wavelength range. The coupled-cavity chain was excited through an adiabatically tapered access waveguide and PhC W1 waveguide in a so-called in-line configuration, which typically allows for high transmission through the resonator chain.[3]

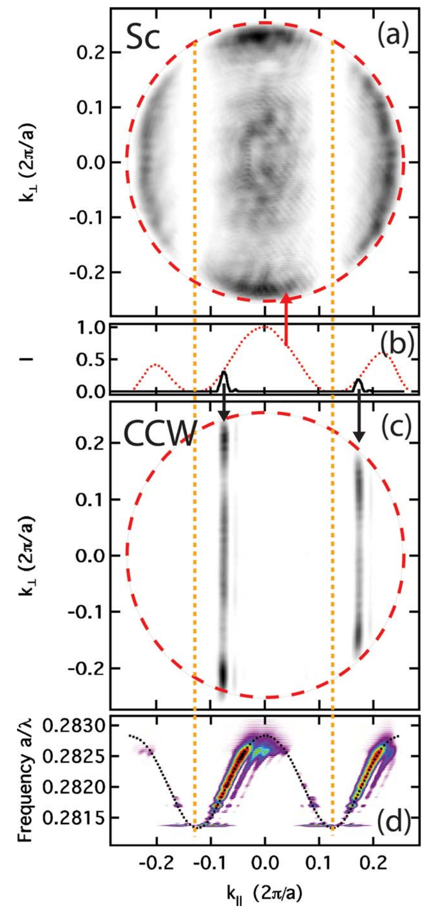

FIG. 2. (Color online) [(a) and (c)] Experimentally measured far-field spectrum of a SC L3 and a CCW formed by 20 cavities, respectively. (b) One-dimensional intensity profile of [(a) and (c)] at $k_\perp=0$. (d) Dispersion curve of the CCW mode.

The actual devices were fabricated on a 220 nm thick silicon-on-insulator wafer with a 2 μm buried oxide layer supplied by SOITEC. After patterning in ZEP-520A positive-tone e-beam photoresist with a resolution of 2.5 nm using Vistec e-beam lithography writer, direct pattern transferring from the ZEP to the Si core layer was performed using Alcatel-AMS200 inductively coupled plasma etching with a SF6-based gas combination.[10] Finally, the 2 μm buried oxide layer was removed with buffered hydrofluoric acid and a supercritical drying was performed to avoid strain in the membrane structure.

To investigate the far-field radiation spectrum of the fabricated devices, we have used a method based on Fourier-space imaging that was already discussed in detail in Ref. 11. The technique uses a high numerical aperture (NA=0.9) lens to collect the light radiated from the sample surface and perform its optical Fourier transform as shown in Fig. 1(c). The resulting Fourier space, or far-field image, which is found in the back-focal plane of the collecting lens, provides us comprehensive information about all spatial components contained in the radiated field.

Figures 2(a) and 2(c) show the measured experimental far-field patterns of an isolated L3 cavity and a CCW, respectively. While the SC radiation pattern extends continuously over the whole pupil of the collecting lens, the spectrum of the CCW is discrete, formed by two narrow lines separated by a distance $2\pi/\Lambda$. Such observation implies that in the direction $r_{\perp}$ perpendicular to the coupled-cavity chain the cavities radiate quasiuniformly such as a SC, while in the propagation direction the emission occurs only at two well-defined angles k and $k+2\pi/\Lambda$. This is in agreement with the theoretical model presented above [Eq. (3)], which predicts the existence of discrete spatial frequencies of the CCW emission.

The absolute position of the spectral lines is determined by the propagation constant of the CCW mode k, which depends on the frequency of excitation ω. When the excitation frequency is tuned, the spectral lines move along the $k_{\parallel}$ axis following the dispersion relation of the coupled-cavity mode. This is shown in Fig. 2(d), where the far-field spectrum integrated along the $k_{\perp}$ axis is plotted as a function of the excitation frequency, yielding the full experimental dispersion curve.[12] However, as the spectral lines move along the dispersion curve, a gradual change of their intensity is observed: the radiated intensity and hence the propagation loss of the CCW reaches its maximum close to the top of the dispersion band and diminishes in the direction toward the first Brillouin zone (BZ) boundary, where it is almost completely suppressed. As follows from both theoretical expression Eq. (3) and the comparison of intensity patterns of Figs. 2(a) and 2(c) [depicted also in Fig. 2(b)], this is a direct consequence of modulation of the CCW far-field spectrum by the emission profile of an isolated cavity. Referring back to Fig. 2(a), the isolated cavity pattern also exhibits a clear maximum at the Γ point and decreases along the $k_{\parallel}$ axis toward distinct minima at approximately $k_{\parallel}/(2\pi/a) = \pm 0.125$, which coincide with the BZ boundary of the coupled-cavity chain.

In our special case, the radiation loss of the investigated CCW decreases as a function of increasing k-vector and frequency. We stress that this conclusion is valid only for the L3 cavity design and low periodicity of the coupled-cavity chain, i.e., $\Lambda=4a$. When the length of the unit cell Λ is increased, the amount of the Bloch mode components lying inside the light cone increases accordingly, which makes the $P_{\mathrm{SC}}(\omega)$ relation more complex. Nevertheless, the wavelength dependent loss of the CCW can be still evaluated using Eq. (3) as the sum of all Bloch mode components lying inside the light cone multiplied by the radiation profile of a single cavity.

Strong variation in the optical loss along the dispersion curve has several consequences on the coupled-cavity device operation. Primarily, it dramatically reduces the transmission bandwidth of the CCW. As illustrated in Fig. 3, only the bottom half of the full CCW bandwidth can be transmitted along the coupled-cavity chain, while for higher frequencies the transmission is completely hindered by excessive radiation loss. If the full bandwidth of the CCW mode is to be used, the radiation profile of the constituent cavities and the periodicity of the CCW must be optimized in order to reduce the waveguide propagation loss below a desired level.

Another detrimental effect of the out-of-plane radiation loss is the renormalization of the dispersion curve in the regime of extreme slow light propagation and consequent limitation of the maximum achievable group index.[13] This is illustrated in Fig. 3, where the experimental dispersion is compared to the theoretical dispersion curve obtained from

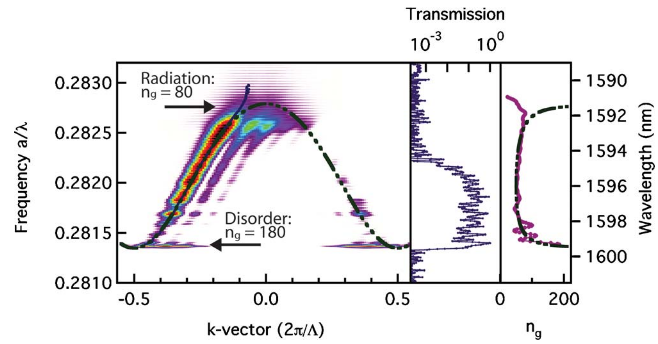

FIG. 3. (Color online) Left: Experimental dispersion curve of the CCW (image plot) compared to the theoretical dispersion calculated by tight-binding approximation (dashed line). Maxima of the experimental data are depicted to better visualize the measured dispersion curve. Middle: Normalized transmission spectrum. Right: Spectral dependence of the group index.

the tight-binding model.[2] At the top of the dispersion band, where the radiation loss dominates, the theoretical group index $n_g=c\times dk/d\omega$ diverges to infinity, while the experimental group index is limited to the value of only $n_g=80$. This discrepancy is attributed to out-of plane radiation loss. Note that at the bottom of the dispersion band where the loss becomes negligible, group index can reach much larger values up to 180 before the light transport gets hindered by structural disorder and related light localization. Hence, suppressing the CCW radiation loss simultaneously pushes the limit of possible light speed reduction, which is important for practical slow-light applications.

To summarize, in addition to the number of Bloch modes lying inside the light cone, the radiation profile of an isolated cavity is a crucial parameter that determines the radiation loss and hence the Q-factor of the CCWs. The optimum choice of the waveguide periodicity Λ can lead to a pronounced suppression of the CCW radiation loss for a specific frequency interval within the CCW bandwidth. However, if the full bandwidth of the CCW mode is to be used, it is the design of the constituent cavities that has to be optimized to efficiently reduce the overall waveguide propagation loss.

The authors acknowledge support from the European projects ePIXnet (Grant No. IST-004525), the MP0702 COST action and the Swiss NCCR-Quantum Photonics.

[1] N. Stefanou and A. Modinos, Phys. Rev. B **57**, 12127 (1998).
[2] A. Yariv, Y. Xu, R. K. Lee, and A. Scherer, Opt. Lett. **24**, 711 (1999).
[3] M. Notomi, E. Kuramochi, and T. Tanabe, Nat. Photonics **2**, 741 (2008).
[4] M. L. Povinelli and S. Fan, Appl. Phys. Lett. **89**, 191114 (2006).
[5] D. P. Fussell and M. M. Dignam, Appl. Phys. Lett. **90**, 183121 (2007).
[6] J. Vučković, M. Lončar, H. Mabuchi, and A. Scherer, IEEE J. Quantum Electron. **38**, 850 (2002).
[7] Y. Akahane, T. Asano, B.-S. Song, and S. Noda, Opt. Express **13**, 1202 (2005).
[8] S. G. Lipson, H. Lipson, and D. S. Tannhauser, *Optical Physics*, 3rd ed. (Cambridge University Press, New York, 1995).
[9] C. A. Balanis, *Anthenna Theory: Analysis and Design*, 3rd ed. (Wiley, Hoboken, 2005).
[10] H. Zhang, M. Gnan, N. Johnson, and R. M. De la Rue, Proceedings of the Integrated Photonics Research and Applications Topical Meeting, Uncasville, CT, 24–26 April 2006 (unpublished).
[11] N. Le Thomas, R. Houdré, M. V. Kotlyar, D. O'Brien, and T. F. Krauss, J. Opt. Soc. Am. B **24**, 2964 (2007).
[12] J. Jágerská, N. Le Thomas, V. Zabelin, R. Houdré, W. Bogaerts, P. Dumon, and R. Baets, Opt. Lett. **34**, 359 (2009).
[13] N. Le Thomas, V. Zabelin, R. Houdré, M. V. Kotlyar, and T. F. Krauss, Phys. Rev. B **78**, 125301 (2008).